ICD Lead Failure Detection through High Frequency Impedance

Daniel T. Kollmann, *Member, IEEE*, Charles D. Swerdlow, MD, Mark W. Kroll, PhD, *Fellow, IEEE*, Gregory J. Seifert, *Member, IEEE*, and Patrick A. Lichter, *Member IEEE*

Abstract— **Abrasion-induced insulation breach is a common failure mode of silicone-body, transvenous, implantable cardioverter defibrillator leads. It is caused either by external compression or internal motion of conducting cables. The present method of monitoring lead integrity measures low frequency conductor impedance. It cannot detect insulation failures until both the silicone lead body and inner fluoropolymer insulation have been breached completely, exposing conductors directly to blood or tissue. Thus the first clinical presentation may be either failure to deliver a life-saving shock or painful, inappropriate shocks in normal rhythm. We present a new method for identifying lead failure based on high frequency impedance measurements. This method was evaluated in 3D electromagnetic simulation and bench testing to identify insulation defects in the St. Jude Medical Riata® lead, which is prone to insulation breach.**

I. Introduction

By increasing years of quality life, implantable cardioverter defibrillator (ICD) systems have revolutionized treatment of life-threatening cardiac arrhythmias. They comprise a generator in a subcutaneous pocket connected to the heart by a multilumen, transvenous lead consisting of a flexible, insulating silicone cylinder with longitudinal lumens through which conductors run from the proximal terminals to small pace-sense electrodes and larger shock coil electrodes. Conductors are surrounded by thin fluoropolymer inner insulating sleeves of polytetrafluoroethylene (PTFE) and ethylene-tetrafluoroethylene (ETFE, Fig. 1) [1, 2].

Designing reliable leads remains a challenge because they must remain inert in the body chemically and tolerate hundreds of millions of flex cycles mechanically. Silicone is flexible, biostable, and biocompatible; but it is prone to abrasion [1, 2]. Historically, outside-in abrasion from constant compressive loads in the pocket has been the most common mechanism of lead failure [3]. More recently, the Riata® lead (St. Jude Medical) was withdrawn from sales in November 2011. In addition to outside-in abrasion, Riata is prone to inside-out abrasion from cyclical compression of silicone against cables, which may cause cables to protrude outside the lead body (externalize) [4]. Inside-out abrasions have also has been reported with other defibrillation lead models that remain in use and pacing leads [5-7].

Present lead-failure diagnostics utilize low-frequency impedance measurements and measures of oversensing [2, 8, 9]. They cannot diagnose insulation breaches until both silicone and inner ETFE insulation have been breached completely [4]. Further, even low-frequency measurement of impedance during high-voltage shocks cannot detect silicone breaches with intact ETFE [10]. Thus a high fraction of failures present clinically with serious consequences including painful shocks, failure to pace, and shorts that abort life-saving shocks and may cause catastrophic generator failure [11]. Despite nominal impedance values during low-voltage measurement pulses, high-voltage shocks may short in either "outside-in" abrasions[12, 13] or "inside-out" abrasions.[14, 15] Further, externalized cables my cause thromboembolic complications despite intact ETFE [16]. A better measurement tool for in-situ ICD lead integrity assessment is needed to detect insulation failures before adverse events occur.

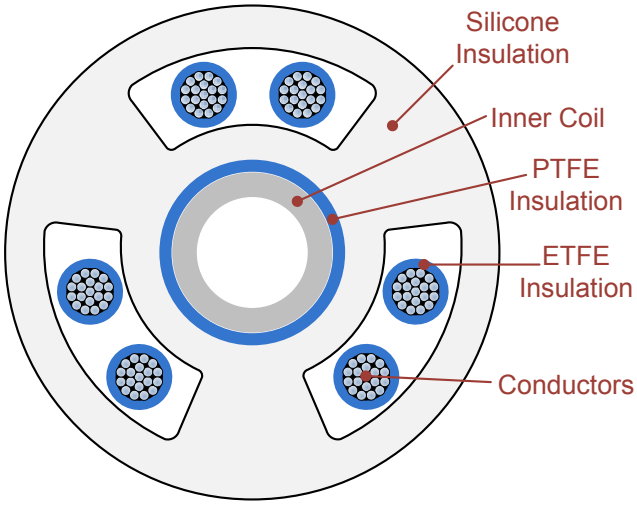

Figure 1. Cross-sectional view between the connector and the SVC electrode of a Riata 8F lead with dual shocking coils. Multiple layers of insulation are used to protect inner conductors including silicone, ethylene-tetrafluoroethylene (ETFE), and polytetrafluoroethylene (PTFE).

Because silicone abrasion alters capacitance between underlying cables and the surrounding blood, we hypothesized that insulation breaches with intact ETFE could be detected by high frequency impedance measurements of

*Research supported by the National Heart, Lung, and Blood Institute grant: 1R43HL120529-01.

D. T. Kollmann and P. A. Lichter are with Koronis Biomedical Technologies, Inc. Maple Grove, MN, 55369, USA.

C. D. Swerdlow is with Cedars-Sinai Heart Center at Cedars-Sinai Medical Center, Los Angeles, CA 90048, USA.

M. W. Kroll is with the Biomedical Engineering Department, University of Minnesota, Minneapolis, MN, 55455, USA and is in the St. Jude Medical speaker's bureau.

G. J. Seifert is with Advanced Medical Electronics, Corp. Maple Grove, MN, 55369, USA.

lead conductors. This study utilized high frequency impedance measurements to observe the effects of insulation failure in both electromagnetic (EM) simulations and direct bench top measurements on leads submerged in a tissue phantom.

II. Lead Failure Modeling

A CAD model of the Riata lead was developed and simulated in CST Microwave Studio [17] to investigate the high frequency impedance profile through 3D EM simulation. This model utilized the entire lead geometry of a 65-cm, dual-coil Model 1580 Riata lead with 17 cm inter-coil spacing, including input connectors, pacing tip and ring electrodes, superior vena cava (SVC) and right ventricular (RV) shock coils, and the lead body. Additional connector and transmission line impedances measured on a test board were included in the model to align the simulation with the bench test. The distal 55 cm of the lead down to the tip electrode is embedded within a rectangular blood phantom to simulate the environment within the vasculature and heart while the proximal 10 cm is surrounded by air to mimic the experimental set up. Dielectric and conductor properties matching the Riata lead construction are assigned to individual components and then a specialized simulation mesh is generated with optimizations to address the relatively long lead length with sufficient resolution for the thin insulation layers and small cable dimensions.

The model is simulated using the Transient Solver within CST Microwave Studio over a 50 – 500 MHz bandwidth with total mesh size exceeding 15 million cells. This solver injects a shaped pulse into the lead input and calculates the resulting 3D electromagnetic fields at discrete time steps in the lead and surrounding medium. In each simulation, a single electrode is measured against all other electrodes as the reference. The 3D EM field response to the injected pulse is post processed to determine the S_{11} input reflection magnitude S-parameter.

S_{11} is a common measurement of 1-port RF circuits and is an indication of impedance mismatch between the load (ICD lead) and a signal generator with 50 ohm source impedance (network analyzer). Changes in real and imaginary load impedance cause a change in S_{11} magnitude and phase. RF equipment typically measures S_{11} using power input and power reflection measurements since it is difficult to accurately measure voltage and current at RF frequencies. The relationship between S_{11} and the lead input impedance Z_{in} is provided in Eq. 1.

$$S_{11} = \frac{Z_{in} - 50}{Z_{in} + 50} \qquad (1)$$

Fig. 2 shows the simulated S_{11} input reflection magnitude S-parameter calculated with a 50 Ω source impedance driving the lead. The 3 conditions simulated are: 1) baseline intact lead, 2) outer silicone removed above RV coil cable, and 3) RV coil cable exteriorized from the lead body. The silicone breach is 3 cm long and is centered at 9.5 cm from the lead tip electrode. A significant change in RV shock coil impedance is observed near 250, 300, and 400 MHz by the large shift in S_{11} magnitude at these frequencies. Ring electrode impedance shifts after removal of silicone insulation over the ring cables are also identifiable in EM simulation along with shorter externalized lengths.

III. Experimental Methods and Results

Experimentally, the ability to detect insulation failure through high frequency impedance changes was evaluated using Model 1580 Riata leads placed in a blood-simulating phantom. Measurements were obtained using a network analyzer (N5242A PNA-X, Agilent Technologies).

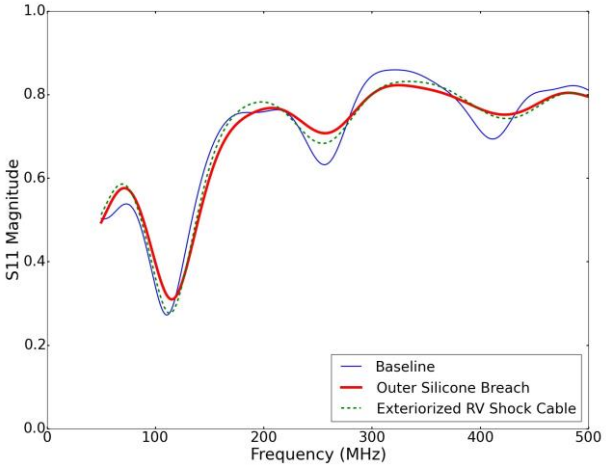

Figure 2. Simulated S_{11} parameter magnitude of the RV shock coil for the baseline intact lead compared to an outer insulation defect for the RV cable with and without exteriorized cable.

A. Blood Simulating Phantom

A recipe was developed for a liquid phantom that simulates the dielectric properties of blood was developed for 50 – 500 MHz. Multiple recipes containing distilled water, salt, and sugar were mixed and tested using an Agilent 85070E dielectric probe connected to a network analyzer. This probe calculates dielectric properties using an open ended coaxial approach with the probe end submerged in the target liquid.

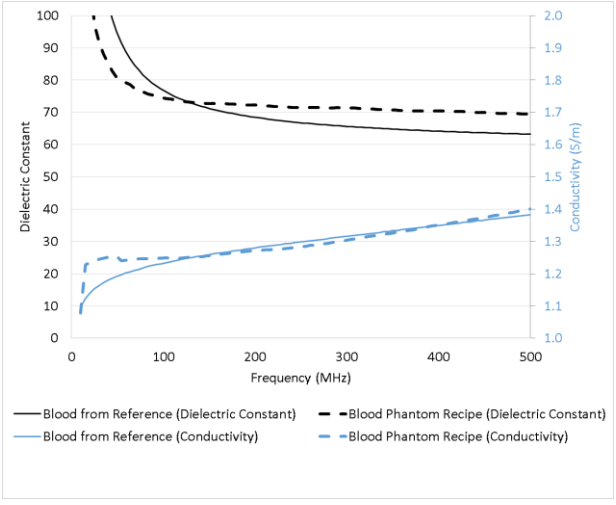

Figure 3. Dielectric constant (top traces) and conductivity (bottom traces) for blood based on reference measurements [19] and with the blood phantom recipe developed in this work.

The selected recipe consists of the following ingredients by weight: 74.92% distilled water, 1.35% NaCl, and 23.73% sugar. Fig. 3 shows the dielectric constant and conductivity for the blood phantom recipe compared to the published properties of human blood.[19] The reference data represents dielectric properties at 37° C while the blood-phantom data is measured at 23° C to align with the bench testing conditions. The recipe matches the dielectric constant within ± 10% over 63 – 500 MHz and the conductivity within ± 10% over 10 – 500 MHz.

B. Test Setup

To ensure repeatable connections to the lead terminals, impedance was measured through a custom lead measurement board (Fig. 4) connected to a network analyzer (N5242A PNA-X, Agilent Technologies). The board utilizes a 4:1 RF switch to connect the input network analyzer RF signal to 1 of 4 lead electrodes. All other lead electrodes are grounded together through the RF switch. A 1-port short, open, and load calibration was performed on the test board between the RF switch and the input cable to remove extra impedance from the coaxial cable connected to the network analyzer.

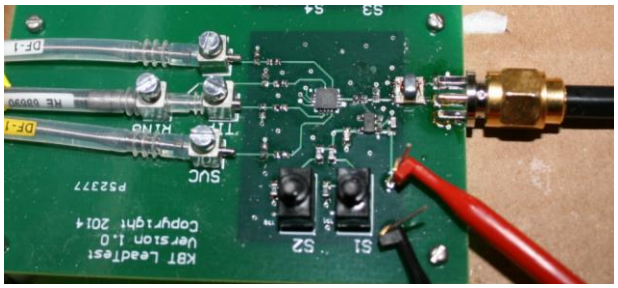

Figure 4. Lead measurement board with 4:1 RF switch, coaxial input connection, and ICD defibrillator lead connector terminals.

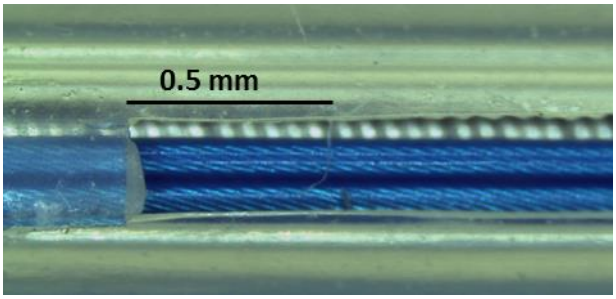

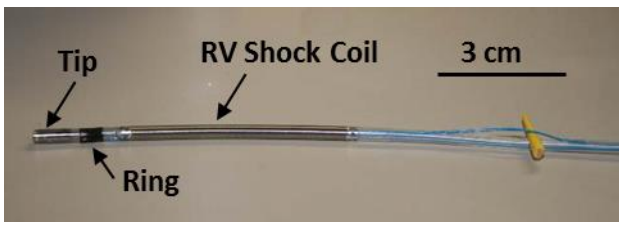

Figure 5. Top: Outer silicone insulation breach with complete removal silicone above the RV shock coil cable. Bottom: Exteriorized RV shock coil cable after outer silicone insulation breach. The cable is held out from the lead body using a wooden toothpick.

Each lead is centered within a 55 cm long by 33 cm wide tub filled to a height of 20 cm with the blood-simulating phantom. The leads were situated in the middle of the tub and elevated 10 cm from the bottom. Leads were positioned straight along the long edge with minimal bends.

C. Lead Impedance Test Cases

RV shock coil high frequency impedance was evaluated under 4 test conditions corresponding to those used in modeling along with a repeat of baseline: 1) baseline with intact lead, 2) repeat baseline after removing lead from the test tub and then repositioning it, 3) outer silicone removed above RV coil cable (Fig. 5 top), and 4) RV coil cable exteriorized from the lead body (Fig. 5 bottom). A scalpel was used under a microscope to remove only silicone without damaging the cable's ETFE coating. Uniform exteriorization was achieved by inserting a small toothpick between the RV coil cable and the lead body. As in simulation, the 2 injury test cases used a 3 cm long insulation defect proximal to the RV shock coil. The defect was centered 9.5 cm from the tip electrode, where insulation failures typically occur [18].

D. Test Results

High frequency impedances were measured from 50 – 500 MHz for 9 leads in the blood simulating liquid. All leads demonstrated a shift in impedance from the baseline measurement with intact insulation to the measurements with silicone insulation damage. A typical S_{11} magnitude plot is shown in Fig. 6. Similar to the simulation, the measured results demonstrated shifts in the following bands: 220 – 250 MHz, 290 – 310 MHz, and 390 – 410 MHz. The impedance shifts are the result of the increase in capacitance between the RV shock coil cable and the surrounding blood at the insulation breach site. This increased capacitance adds in parallel to the RV shock coil impedance, effectively changing the impedance match to the 50 ohm input source signal.

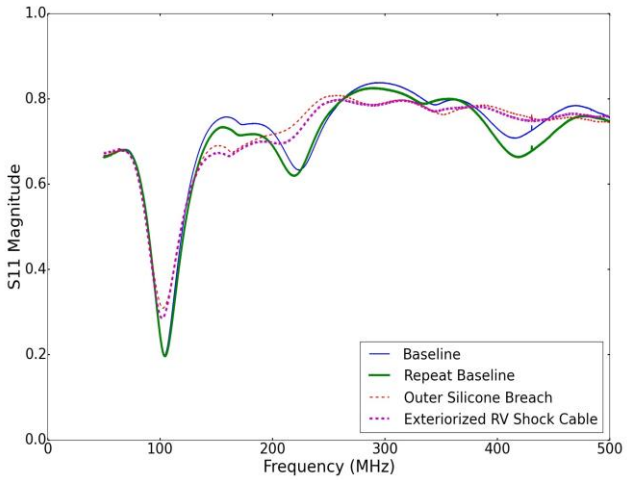

Figure 6. Measured S_{11} parameter magnitude of the RV shock coil for the baseline intact lead compared to an outer insulation defect for the RV shock coil cable with and without exteriorized cable.

Table 1. Frequency bands with significant ($p < 0.01$) change in measured S_{11} magnitude mean ($n = 9$). P values are relative to the baseline measurement.

Frequency Band (MHz)	*Baseline S_{11} Magnitude*	*Outer Silicone Breach S_{11} Magnitude*	*Exteriorized RV Coil Cable S_{11} Magnitude*
220 – 250	0.671 ± 0.034	0.727 ± 0.039, p = 0.0002	0.728 ± 0.030, p = 0.0002
290 – 310	0.815 ± 0.014	0.770 ± 0.023, p = 0.0001	0.758 ± 0.022, p = 0.0001
390 – 410	0.727 ± 0.030	0.755 ± 0.027, p = 0.0074	0.757 ± 0.022, p = 0.0016

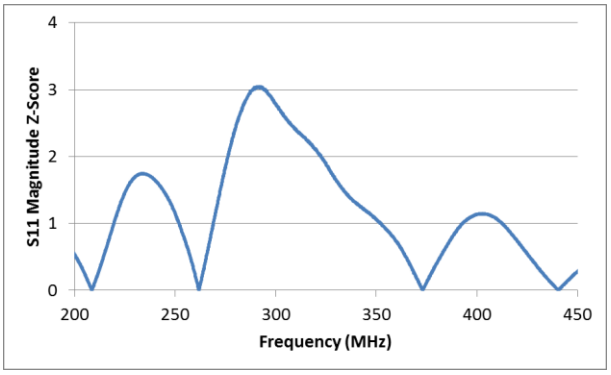

Figure 7. Measured S_{11} magnitude Z-Score for statistical comparison between the baseline leads and the two injured groups combined.

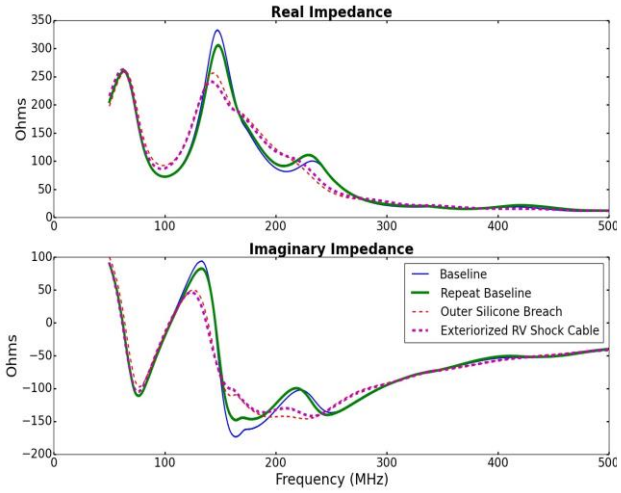

Figure 8. Real and imaginary impedance for the RV shock coil in the baseline intact insulation and repeat baseline test cases compared to an outer insulation defect for the RV shock coil cable with and without exteriorized cable.

A longitudinal panel analysis was run on the S_{11} magnitudes for the baseline and injured lead conditions. This analysis identified 3 frequency bands with statistically significant ($p < 0.01$) changes in mean S_{11} magnitude between the baseline intact leads and the damaged leads: 220 – 250 MHz, 290 – 310 MHz, and 390 – 410 MHz. The S_{11} magnitude samples were conservatively averaged across each frequency band for the test conditions and the results are listed in Table 1. The S_{11} magnitude mean Z-Score

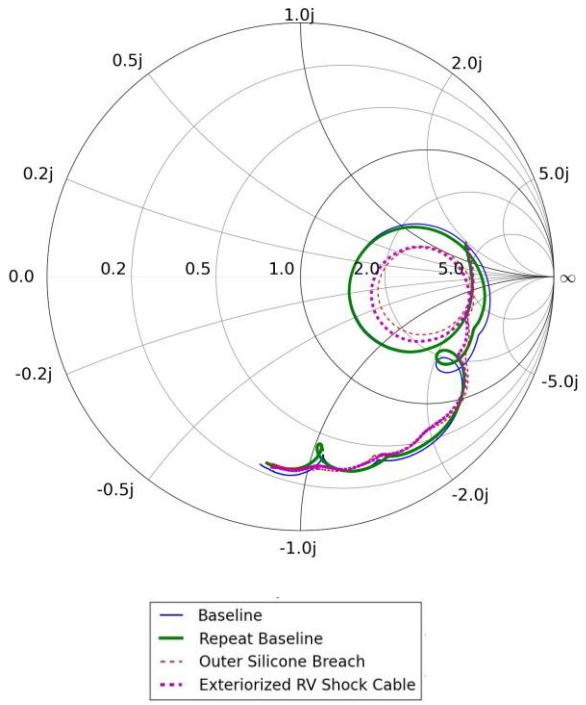

Figure 9. Smith chart format of the measured S_{11} parameter for the RV shock coil in the baseline intact insulation and repeat baseline test cases compared to an outer insulation defect for the RV shock coil cable with and without exteriorized cable.

(difference in means divided by the standard deviation) vs. frequency shown in Figure 7 was calculated through a comparison of a combined baseline and repeat baseline group to a combined outer silicone breach and exteriorized RVC cable group. Frequency ranges with elevated Z-Score indicate statistically significant shift in S_{11} magnitude between the baseline and injured leads.

Fig. 8 shows the RV shock coil impedance for a single lead plotted in real and imaginary format. The same data is shown in Smith chart format in Figure 9, which displays both the real and imaginary impedance across a frequency range. Each inner circle labeled on the middle line denotes a constant range of real impedances with the real impedance increasing from the left side of the outer circle to the right side of the outer circle. The top half of the Smith chart represents positive imaginary impedances (inductive) while the lower half represents negative imaginary impedances (capacitive). Axis markers are equal to the impedance normalized to 50 ohms. This plot format shows the RV shock coil impedance varies significantly across the 50 – 500 MHz frequency range appearing as either inductive or capacitive depending on the frequency, similar to the behavior of a transmission line loaded with an impedance mismatch. The impact of insulation breach is notable in the middle of the plot. The breach reduces the range between the minimum and maximum for both real and imaginary impedance, seen as a reduction in radius of the circle trace. Separate plots of S_{11} magnitude for each individual lead are included in Fig. 10.

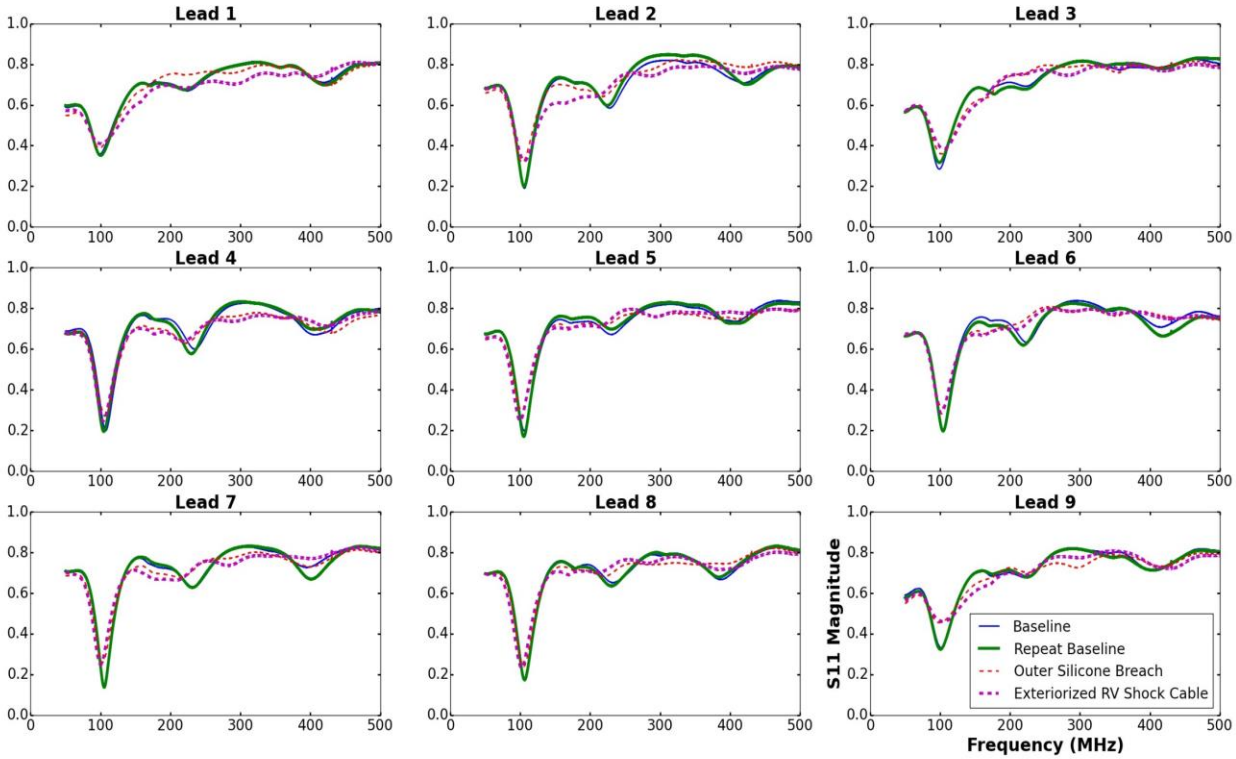

Figure 10. Measured RV shock coil S_{11} parameter magnitude for all 9 tested leads.

IV. Conclusion

High frequency impedance measurements detect breaches of outer silicone insulation in ICD leads that elude detection by clinically-used lead diagnostics. This method has the potential to identify subclinical insulation breaches in leads implanted in patients, thus preventing serious adverse outcomes. Good agreement between modeling and bench testing allows rapid investigation of additional defect parameters including breach length and location. Future work will evaluate the predicted impact of silicone breach on ring-electrode impedance and extend this technique to other lead failure modes, such as conductor fracture.

Limitations

This study used new leads that were in a dry state. Fluid ingress may change the frequency signature of chronically implanted leads. Also, we did not study the effects of the lead curvature in the vascular system, coiling in the pocket, or variations in the length of the proximal lead section exposed to air.

Acknowledgment

The authors thank St. Jude Medical for their support in providing ICD lead test samples and ICD lead construction details. We also thank James Brewer, MS for his statistical analysis of the lead measurements.

References

[1] H. M. Haqqani and H. G. Mond, "The implantable cardioverter-defibrillator lead: principles, progress, and promises," *Pacing and Clinical Electrophysiology*, vol. 32, pp. 1336-53, Oct 2009.

[2] C. D. Swerdlow and K. A. Ellenbogen, "Implantable cardioverter-defibrillator leads: design, diagnostics, and management," *Circulation,* vol. 128, pp. 2062-71, 1-9, Oct 29 2013.

[3] T. Kleemann, T. Becker, K. Doenges, M. Vater, J. Senges, S. Schneider*, et al.*, "Annual rate of transvenous defibrillation lead defects in implantable cardioverter-defibrillators over a period of >10 years," *Circulation,* vol. 115, pp. 2474-80, May 15 2007.

[4] R. G. Hauser, D. McGriff, and L. K. Retel, "Riata implantable cardioverter-defibrillator lead failure: analysis of explanted leads with a unique insulation defect," *Heart Rhythm,* vol. 9, pp. 742-9, May 2012.

[5] C. D. Swerdlow, R. M. Kass, A. Khoynezhad, and S. Tang, "Inside-out insulation failure of a defibrillator lead with abrasion-resistant coating," *Heart Rhythm,* vol. 10, pp. 1063-6, Jul 2013.

[6] U. Lakshmanadoss, V. Hackett, and P. Deshmukh, "Externalized Conductor Cables in QuickSite Left Ventricular Pacing Lead and Riata Right Ventricular Lead in a Single Patient: A Common Problem With Silicone Insulation," *Cardiology Research,* vol. 3, pp. 230-231, 2012.

[7] J. A. Manfredi, S. M. Smithgall, C. M. Kircher, and M. A. Lollis, "Insulation failure with externalized conductor of a linox sd lead: A case report," *Journal of Cardiovascular Electrophysiology,* 2014.

[8] L. M. Kallinen, R. G. Hauser, K. W. Lee, A. K. Almquist, W. T. Katsiyiannis, C. Y. Tang*, et al.*, "Failure of impedance monitoring to prevent adverse clinical events caused by fracture of a recalled high-voltage implantable cardioverter-defibrillator lead," *Heart Rhythm,* vol. 5, pp. 775-9, Jun 2008.

[9] C. D. Swerdlow, B. D. Gunderson, K. T. Ousdigian, A. Abeyratne, H. Sachanandani, and K. A. Ellenbogen, "Downloadable software algorithm reduces inappropriate shocks caused by implantable cardioverter-defibrillator lead fractures: a prospective study," *Circulation,* vol. 122, pp. 1449-55, Oct 12 2010.

[10] A. Fischer and R. Klehn, "Contribution of ethylenetetrafluoroethylene (ETFE) insulation to the electrical performance of Riata® silicone leads having externalized conductors," *Interventional Cardiac Electrophysiology,* vol. 37, pp. 141-5, Aug 2013.
[11] R. K. Sung, B. M. Massie, P. D. Varosy, H. Moore, J. Rumsfeld, B. K. Lee*, et al.*, "Long-term electrical survival analysis of Riata and Riata ST silicone leads: National Veterans Affairs experience," *Heart Rhythm,* vol. 9, pp. 1954-61, Dec 2012.
[12] J. N. Catanzaro, J. A. Brinker, S. K. Sinha, and A. Cheng, "Abrasion of a DF-4 defibrillator lead," *Cardiovascular Electrophysiology,* vol. 24, pp. 718-719, Jan 31, 2013 2013.
[13] D. P. Leong and L. van Erven, "Unrecognized failure of a narrow caliber defibrillation lead: the role of defibrillation threshold testing in identifying an unprotected individual," *Pacing and Clinical Electrophysiology,* vol. 35, pp. e154-5, Jun 2012.
[14] R. H. Abdelhadi, S. F. Saba, C. R. Ellis, P. K. Mason, D. B. Kramer, P. A. Friedman*, et al.*, "Independent multicenter study of Riata and Riata ST implantable cardioverter-defibrillator leads," *Heart Rhythm,* vol. 10, pp. 361-5, Mar 2013.
[15] P. Shah, G. Singh, S. Chandra, and C. D. Schuger, "Failure to deliver therapy by a Riata Lead with internal wire externalization and normal electrical parameters during routine interrogation," *Cardiovascular Electrophysiology,* vol. 24, pp. 94-6, Jan 2013.
[16] S. K. Goyal, C. R. Ellis, J. N. Rottman, and S. P. Whalen, "Lead thrombi associated with externalized cables on Riata ICD leads: a case series," *Cardiovascular Electrophysiology,* vol. 24, pp. 1047-50, Sep 2013.
[17] CST Microwave Studio. Available at: https://www.cst.com/Products/CSTMWS. Accessed March 17, 2014.
[18] K. A. Ellenbogen, C. D. Swerdlow, J. Rhude, R. Williamson, A. Dianaty, A. Fischer. "Sites of insulation abrasion and exposed cable conductors in Riata and Riata ST silicone leads: Analysis from extracted leads," *Heart Rhythm* S119, PO01-77, 2013.
[19] C. Gabriel, "Compilation of the Dielectric Properties of Body Tissues at RF and Microwave Frequencies", Brooks Air Force Technical Report AL/OE-TR-1996-0037, 1996.